Arabian Journal of Geosciences (2021) 14: 1
https://doi.org/10.1007/s12517-020-06304-8

ORIGINAL PAPER

Effect of soil microstructure on the small-strain shear modulus of saline soil

Xingang Wang[1,2] · Tangdai Xia[1] · Longju Zhang[2] · Zhi Ding[3] · Shaoheng He[1] · Yu Peng[1]

Received: 3 August 2020 / Accepted: 28 November 2020 / Published online: 6 January 2021

Abstract

The behavior of soils at small strains ($< 10^{-5}$) is of significant interest for geotechnical engineers. Compared with the small-strain properties of sand or clay, those of saline soil have been investigated less extensively and therefore remain poorly understood. Accordingly, this study investigates the influence of microstructure on the small-strain shear modulus (G_0) of saline soil. A series of specifically designed experiments was conducted on saline soil specimens under unsaturated conditions via the resonant column technique and scanning electron microscopy. The results showed that the G_0 of saline soil increases with the dry density. The obtained values of the fitting parameter, A, are between 52.06 and 63.42, with an average value of 58.82, while those of the fitting parameter, n, are between 0.284 and 0.363, with an average value of 0.322. The Na_2SO_4 content was employed as a state variable, using which Hardin's equation was modified for proper consideration of the influence of the Na_2SO_4 content on the prediction of G_0. The results show that G_0 increases with the Na_2SO_4 content. The inflection point of the Na_2SO_4 content with a significant change in G_0 is 20%. The main contact forms of soil particles are edge–edge, edge–surface, and surface–surface contacts. With increasing Na_2SO_4 content, the cementation of soil particles by salt crystals gradually replaces the inter-particle contact, and sulfate crystal cementation becomes the dominant factor affecting G_0.

Keywords Salinized soil · Shear modulus · Microstructure · Resonance column test · SEM image

Introduction

Saline soil is a special type of soil that contains a certain amount of salt and is widely distributed in western China. Saline soil covers an area of up to 4.583×10^7 hm^2 in Xinjiang, accounting for 9.5% of the local available land area (Xu 1993). Owing to its unique soil components and the high sensitivity of its engineering properties to water and temperature, saline soil has been considered problematic, which has been the focus of extensive research activities.

The microstructure of soil determines its macro-performance. Thus, the special physical and engineering properties of saline soil are also determined by its microstructure. The particle size and shape are the most important microstructural parameters, as these determine the pore distribution, particle connection, and particle arrangement (Al-Mukhtar et al. 2012; Gao et al. 2018). The microstructure of saline soil has been analyzed by several scholars (Li et al. 2016; Liu and Zhang 2014). To elucidate the relationship between the Na_2SO_4 content and the small-strain shear modulus (G_0), scanning electron microscopy (SEM)

Responsible Editor: Zeynal Abiddin Erguler

✉ Longju Zhang
1158765469@qq.com

Xingang Wang
11712036@zju.edu.cn

Tangdai Xia
xtd@zju.edu.cn

Zhi Ding
dingz@zucc.edu.cn

Shaoheng He
heshaoheng@zju.edu.cn

Yu Peng
zjupengyu@zju.edu.cn

[1] College of Architectural Engineering, Zhejiang University, Hangzhou 310012, China

[2] College of Water Conservancy and Architectural Engineering, University of Tarim, Alar 843300, China

[3] Zhejiang University City College, Hangzhou 310015, China

Table 1 Physical properties of saline soil

Liquid limit	Plastic limit	Liquid index	Particle size (mm)					Effective particle size	Particle density	Coefficient of nonuniformity	Curvature coefficient
			> 0.25	0.25~0.075	0.075~0.005	< 0.005	< 0.002				
W_l	W_p	I_p	content(%)					d_{10}	G_s	C_u	C_c
%		–						mm	g/cm^3	–	–
31.8	19.8	12	–	6	66.5	27.5	14	0.0013	2.65	14.2	1.6

images of the saline soil pore structure have been analyzed both qualitatively and quantitatively.

Resonant column tests are commonly conducted to investigate the dynamic properties of soils. This method was popularized by scientists such as Hall and Richart in 1963; Drnevich et al. 1967; and Hardin and Black in 1968 (Hall Jr and Richart Jr 1963; Drnevich et al 1967; Hardin and Black 1968). The dynamic shear modulus and damping ratio are two important parameters considered when describing soil dynamic characteristics (Senetakis et al. 2013). These parameters are required to build the Hardin–Drnevich (Hardin and Drnevich 1972) model, which describes the stress–strain relationship (Nie et al. 2008;Liu et al. 2019). However, experimental investigations of the small-strain shear modulus and damping ratio of saline soil have received considerably less attention than the efforts focused on other soil types. Many of the previous experimental investigations of the dynamic properties of soils have focused on sand, clay, and loess (Wichtmann and Triantafyllidis 2009, 2013). Jafarian studied the dynamic properties of calcareous and siliceous sands under the conditions of isotropic and anisotropic stress (Jafarian et al. 2014). Dutta investigated the effect of saturation on the shear modulus (G_0) and damping ratio (D) of compacted clay through a series of resonant column tests; it was concluded that G_0 decreased and D increased with increasing saturation (Dutta et al. 2017). Presti explored the effect of the strain level, loading rate, number of loading cycles, and type of loading on the variation in G_0 and D in two natural clays through a series of resonant column tests (Presti et al. 1997). However, few studies have reported on the dynamic properties of saline soil. In the near future, under the guidance of the Belt and Road Initiatives, southern Xinjiang is expected to invest hundreds of billions to build several major road projects. In addition, Xinjiang experiences a high earthquake frequency and intensity, with large-magnitude earthquakes occurring over a wide range. Therefore, it is necessary to study the microstructure and dynamic characteristics of the saline soil in this area.

In this study, the influence of the dry density and Na_2SO_4 content on the G_0 of saline soil was investigated through resonance column tests and X-ray diffraction analyses. SEM experiments were carried out on saline soils with different Na_2SO_4 contents to reveal the influence of the sulfate content on G_0 on a microscopic scale. The results of this study can provide an important reference for engineering practice in regions with saline soil.

Materials and methods

Study area and soil properties

Southern Xinjiang is an area with an arid continental desert climate; it has a dryness of greater than 2.0, annual average

Table 2 Test results of soil salt-based ions

Sampling depth	Cl^-	CO_3^{2-}	HCO_3^-	SO_4^{2-}	Ca^{2+}	Mg^{2+}	K^+	Na^+	Total soluble salts	PH value
m	g/kg									–
0–0.2	3.067	–	0.11	1.2	1.4	0.45	6.69	7.615	20.53	8.26

precipitation of 69.2–147.2 mm, and an annual average evaporation of 2175.7–2408.3 mm. Salt in the groundwater and soil migrates and accumulates to a certain thickness on the surface through capillary action, resulting in severe soil salinization. Chloride and sulfuric acid in salinized soil are widely distributed, and the salt content in some areas is as high as 20–100 g/kg. Chlorine saline soil is white and cool on the tip of the tongue, while sulfate saline soil is brown-yellow and bitter on the tip of the tongue.

The saline soil in this study was sampled in Alar city, Xinjiang, China, located in the north of the Taklimakan Desert. Brown-yellow saline soil samples were taken at depths of 0–30 cm; the groundwater depth was 1.3 m. Basic parameters and the particle size distribution of the saline soil samples are listed in Table 1. The base ion content is presented in Table 2. The basic parameters were determined according to the Chinese standard for soil test methods (GB/T 50123-2019). According to the chemical composition classification equation of salt (Eq. 1), the saline soil is a chlorine saline soil:

$$\omega = \frac{c(Cl^-)}{2c\left(SO_4^{2-}\right)} \quad (1)$$

Fig. 1 GDS resonant column apparatus with specimen

where c indicates the content of Cl^- and SO_4^{2-} in millimoles. Based on the salt content, the soil sample is a medium saline soil.

Resonant column test

GDS resonant column apparatus is used in these experiments (Fig. 1) and consists of a triaxial cell and a strictly restricted base pedestal. During the resonant column tests, specimens can be examined under dry, semi-saturated, or fully saturated conditions with a height-to-diameter ratio of 2:1. The top active end of the specimen is attached to an excitation source consisting of two magnets surrounded by four coils, for torsional loading, and one magnet with one coil for longitudinal loading.

The specimen is 50 mm in diameter and 100 mm in height. First, dried and ground natural soil and saline soil samples of corresponding quality are weighed on the basis of the dry density and sample volume. Subsequently, the samples are mixed with water to achieve a certain moisture content and stirred evenly. Finally, the mixture is divided into five layers in a sample mold with a height of 20 mm, and the layers are polished with a knife to render them rough and to ensure their uniformity. The resonant column test scheme is summarized in Table 3. In each test, increasing confining pressures are applied to the specimen in steps of 50, 100, 200, 300, and 500 kPa. After the sample is loaded to a specific confining stress level, it is consolidated for 30 min to allow the internal linear variable differential transformer to become stable.

In the process of testing, the cylindrical sample was excited in torsion mode by a driving system, which was consisted of a four-arm rotor and a support cylinder. Theoretical basis of resonant column test is to vibrate the tested specimen in a basic pattern of vibration, and then produces the torsion or flexure. The top-cap was positioned on the top of the sample, and the drive system should be carefully aligned to ensure free movement of each magnet within the coils. Then, specimen was isobarically consolidated until the LVDT was stable. The initial drive voltage was set to 0.008 V, during the test shear strain was controlled between 10^{-6} and 10^{-4}. Based on the resonance frequency, sample density (ρ), geometric dimensions, and boundary conditions of samples, the G_0 was extrapolated by the following equation:

Table 3 Experimental scheme for the resonance column tests and scanning electron microscopy analyses of saline soil

Type of test	Dry density (g/cm^3)	Moisture content (%)	Salt content (%)	Number of specimen
Resonant column test	1.4, 1.45, 1.5, 1.55	17	Natural salt content(20.53 g/kg)	4
	1.5	18	Na_2SO_4 content 2%, 6%, 10%, 15%, 20%, 25%, 30%	7
SEM	1.5	0%	Na_2SO_4 content 2%, 6%, 10%, 15%, 20%, 25%, 30%	12

$$G_0 = \rho\left(\frac{2\pi f l}{\beta}\right)^2 \quad (2)$$

where f is resonance frequency, ρ is sample density, l is sample height (mm), and β is eigenvalue of vibration equation.

Scanning electron microscopy

Electron microscopy can be used to observe the microtexture and microstructure of materials at scales ranging from nanometers to micrometers. In this study, SEM (FEG650) was used to investigate the microstructure and morphology of the saline soil. The microtexture of specimens was observed in grey-level images at × 2000 magnification. The porosity was quantified on the basis of binary images, which were obtained by thresholding the grey-level. For dealing with the grey-level images at × 2000 magnification, Image-Pro Plus (IPP), a commercial software developed for image processing, was used to threshold and count the number and measure the size of pores. The SEM test scheme is summarized in Table 3.

Quantitative analysis of test result

X-ray diffraction results

The results of the X-ray diffraction (XRD) analyses of the Alar saline soil (Fig. 2) reveal that the primary minerals present are mica, quartz, and chlorite, with a small content of calcite and kaolinite. Sodium sulfate is also detected at a content of 2.2% via the XRD analyses. Quantitative analysis of the mineral composition is carried out using X'Pert HighScore Plus software. The obtained mineral content is as follows: 20.3% quartz, 11% calcite, 6.6% kaolinite, 16.2% chlorite, 29% mica, 14.6% feldspar, and 2.2% Na_2SO_4. Chlorite and mica are flaky minerals that jointly account for 45.2% of the mineral content.

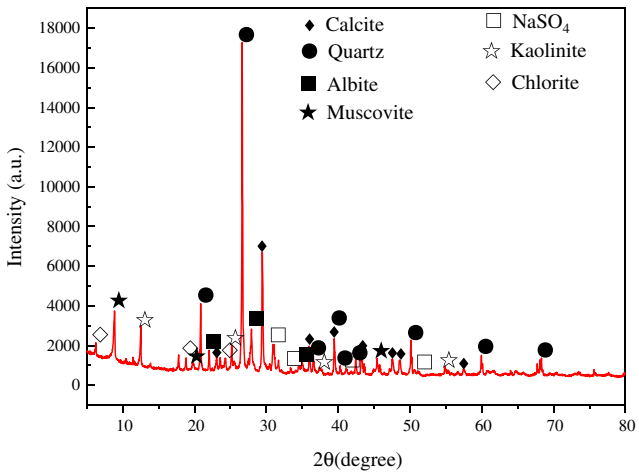

Fig. 2 X-ray diffraction pattern of a salinized soil sample

Shear modulus analysis through resonant column tests

Shear modulus of saline soil under different dry density conditions

The relationships between the shear modulus, G_0, and confining pressure of saline soil specimens under different dry density conditions are shown in Fig. 3. It can be seen from Fig. 3 that the shear modulus increased with the confining pressure, and the growth rate decreased gradually. For the condition of ρ_d = 1.45 g/cm^3 as an example, G_0 increased by 28.91, 15.17, and 8.71 MPa in the range of 0–100 kPa, 100–200 kPa, and 200–300 kPa, respectively.

The shear modulus, G_0, of saline soil is significantly affected by the confining stress (Iwasaki et al. 1978; Kokusho 1980; Tatsuoka et al. 1978). The power function presented in Eq. (3) was initially proposed by Hardin and has been widely used to

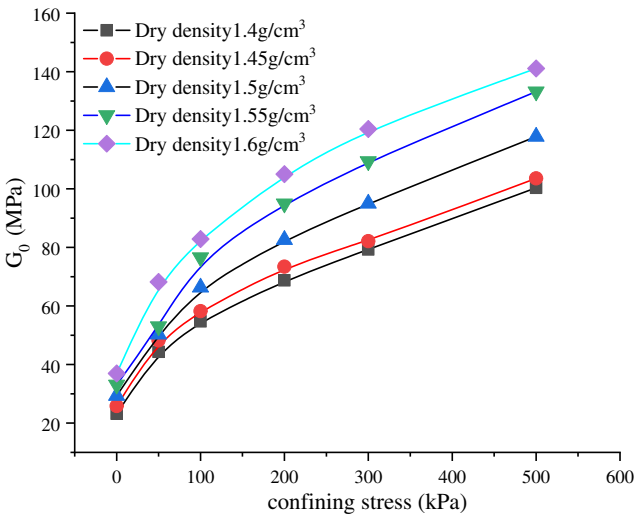

Fig. 3 G_0 at different dry densities

Table 4 Fitting parameters for saline soil

Dry density (g/cm^3)	Best-fit parameters in Eq. (1)		
	A	n	R^2
1.4	63.42	0.284	0.994
1.45	59.35	0.305	0.985
1.5	52.06	0.335	0.997
1.55	58.5	0.363	0.989
1.6	60.75	0.321	0.998

describe the quantitative relationship between the small-strain shear modulus, G_0 (MPa), and the effective mean confining stress:

$$G_0 = AF(e)\left(\frac{\sigma'}{P_a}\right)^n \tag{3}$$

where σ' is the confining pressure; P_a is a reference pressure, usually considered as the atmospheric pressure; and $F(e)$ is a function of the void ratio (e), typically taking the following form (Iwasaki and Tatsuoka 1977):

$$F(e) = \frac{(2.17-e)^2}{(1+e)} \tag{4}$$

Finally, A (in MPa) and n are material constants; the best-fit values for parameters A and n are summarized in Table 4.

As can be seen from Table 4, the fitting parameter A is between 52.06 and 63.42, with an average value of 58.82, and n is between 0.284 and 0.363, with an average value of 0.322. The correlation coefficient R^2 is close to 0.99.

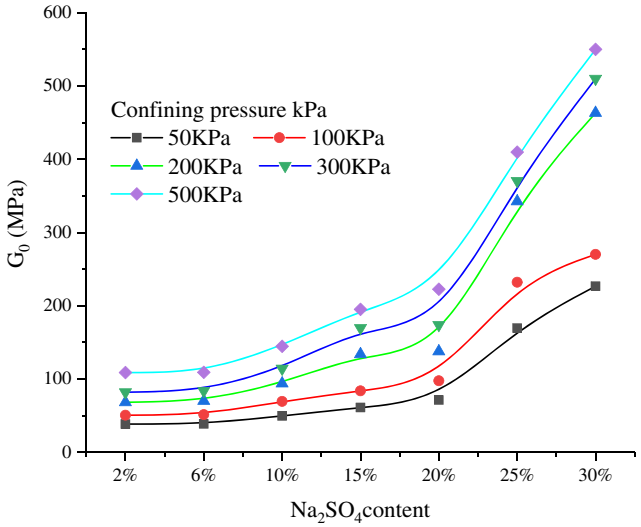

Fig. 4 Relationship between Na_2SO_4 content and G_0

Shear modulus of saline soil with different sodium sulfate contents

Anhydrous Na_2SO_4 is added to natural saline soil to obtain sodium sulfate contents of 2%, 6%, 10%, 15%, 20%, 25%, and 30%. Figure 4 shows the relationship between the shear modulus and Na_2SO_4 content. It can be seen from Fig. 4 that under the same confining pressure, the shear modulus increases gradually with increasing Na_2SO_4 content.

Under confining pressure of 100 kPa, in the range of 2–6%, 6–10%, 10–15%, 15–20%, 20–25%, and 25–30% of Na_2SO_4 content, the increment of shear modulus G_0 is 1.6%, 35.2%, 16.5%, 21%, 16.5%, 137%, and 122%, respectively. According to the trend of the curve in Fig. 4, when the content of Na_2SO_4 is less than 20%, G_0 increases gradually with increasing sodium sulfate content; when the content of Na_2SO_4 is greater than 20%, there is a dramatic increase in G_0.

Among the numerous factors leading to variations in G_0, the confining stress and void ratio are recognized as the most fundamental (Liu et al. 2016; Yang and Liu 2016). G_0 is usually determined using Eq. (2); however, in view of the complexity of crystallization and the change in void ratio after Na_2SO_4 water absorption, the Hardin equation is modified in this study. The modified equation is as follows:

$$G_0 = \alpha F(Na_2SO_4)F(e) + B\left(\frac{\sigma'}{P_a}\right) \tag{5}$$

where $F(Na_2SO_4)$ is the sulfate function. On the basis of the variation in G_0 in saline soils with different sodium sulfate contents, the following sulfate function is proposed:

$$F(Na_2SO_4) = e^{-\theta\omega_{(Na_2SO_4)}} \tag{6}$$

where $\omega_{(Na_2\ SO_4)}$ is the sulfate content. ORIGIN software is used to fit the relationship between the shear modulus and sodium sulfate content. θ, B, and n are fitting parameters, which have values of − 0.1, 26.2, and 0.549, respectively. The values of fitting parameter α are 7.71, 19.3, 17.7, 23.34, and 30.5 at 50, 100, 200, 300, and 500 kPa, respectively. Figure 5a and b shows the fitting of G_0 at different sodium sulfate contents under the same dry density.

SEM microstructure observations

Figure 6a–g show the microstructures of specimens with different Na_2SO_4 contents. In the SEM observations, the skeleton particles of saline soil are mostly sheet- or plate-like aggregates with non-uniform size. This is consistent with the results of the XRD analyses, which indicated that the flaky chlorite and mica minerals comprised 45.2% of the total mineral content. As shown in Fig. 6b and c, certain amounts of salt and fine particles are adsorbed on the surface of the lamellar

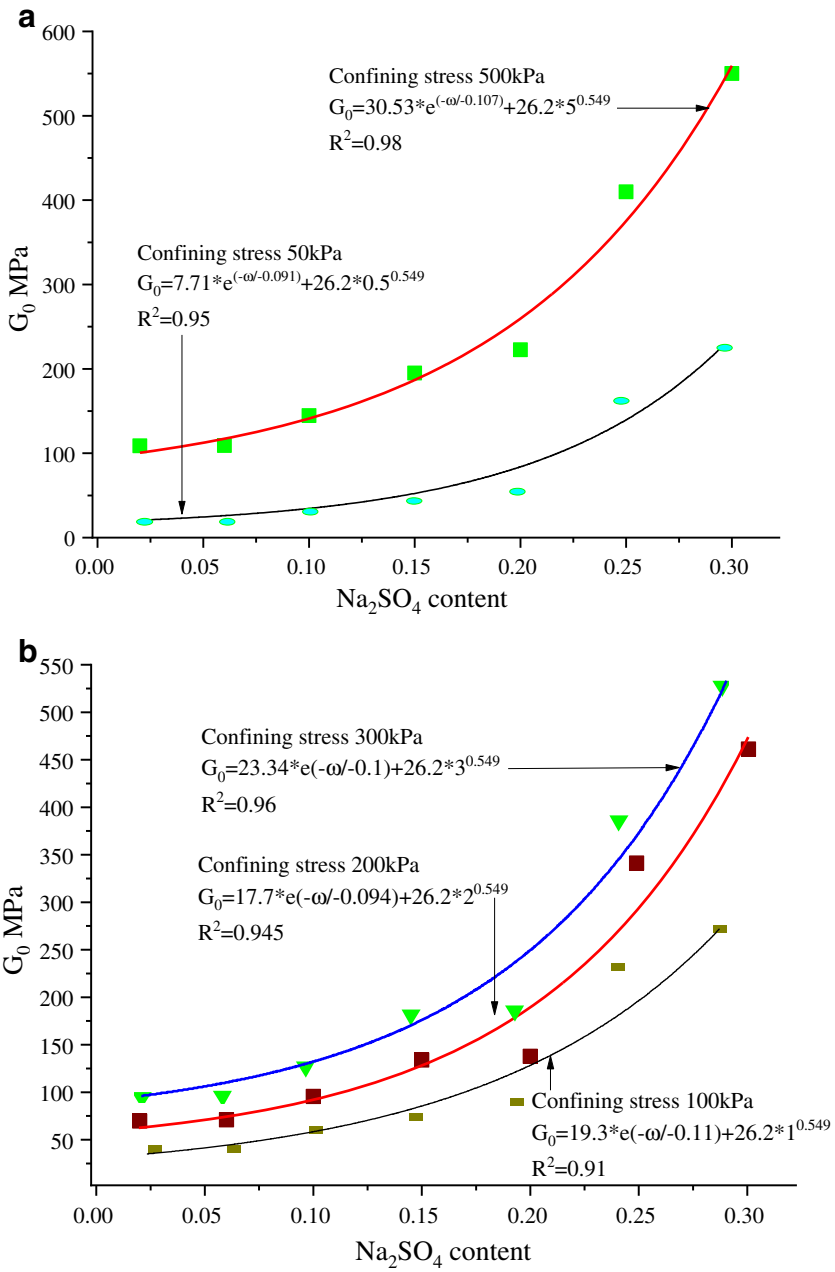

Fig. 5 Fitted relationship between the shear modulus and Na_2SO_4 content. **a** Fit curve of G_0 and Na_2SO_4 content under confining pressure of 50 and 500 kPa. **b** Fit curve of G_0 and Na_2SO_4 content under confining pressure of 100, 200, and 300 kPa

minerals through point–surface contacts. Micropores and tiny cracks are also observed in the saline soil. The sheet-shaped particles have irregular edges, and the skeleton of the soil particles is disordered and loose. The main contact forms are edge–edge, edge–surface, and surface–surface contacts (Fig. 6d). With increasing sodium sulfate content, the amount of Na_2SO_4 crystal particles also increases. When the content of sodium sulfate reaches 20% (Fig. 6e), gray- and white-colored rhombic sodium sulfate crystals can clearly be observed. The form of the connection between the soil particles gradually transforms to sulfate crystal cementation. With increasing sodium sulfate content, the soil particles and Na_2SO_4 crystals become more evenly distributed. With a further increase in the salt content (Fig. 6f and g), the cementation of the salt crystals is enhanced.

Finally, the skeleton structure is formed through the cementation of salt crystals, and a dense skeleton structure with filled soil particles is formed. With increasing Na_2SO_4 crystal cementation, the shear modulus (G_0) increases gradually. At a confining pressure of 50 kPa and the same dry density, the growth rate of G_0 is 1%, 28.5%, 58.5%, 84.6%, 339%, and 443% at sodium sulfate contents of 2%, 6%, 10%, 15%, 20%, 25%, and 30%, respectively.

The image acquisition, processing, and measurement abilities of the IPP software are used to conduct qualitative and quantitative analyses of the SEM images. To achieve the best

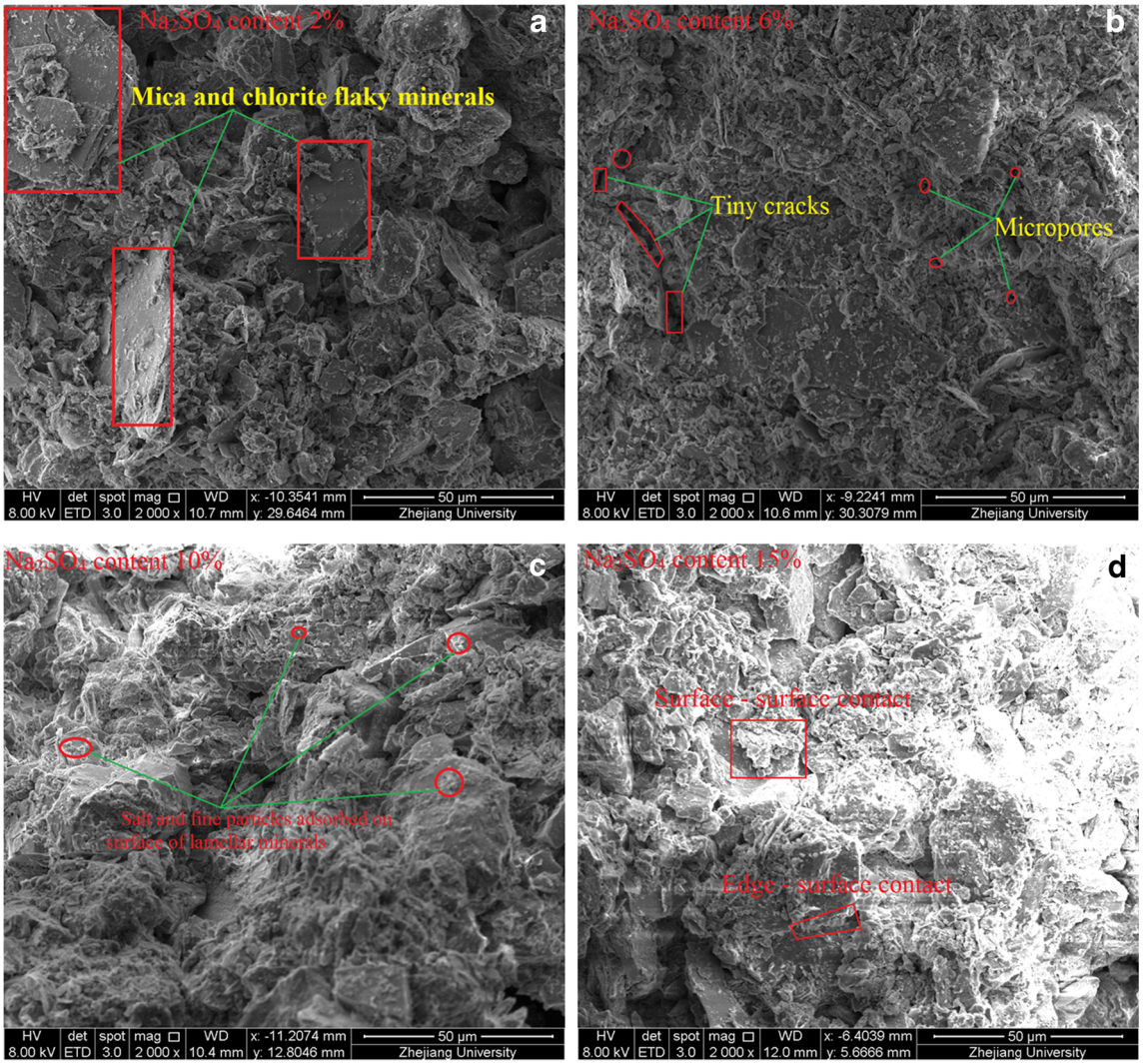

Fig. 6 SEM images of saline soil with different sodium sulfate contents. **a** Na_2SO_4 content: 2%. **b** Na_2SO_4 content: 6%. **c** Na_2SO_4 content: 10%. **d** Na_2SO_4 content: 15%. **e** Na_2SO_4 content: 20%. **f** Na_2SO_4 content: 25%. **g** Na_2SO_4 content: 30%

observation effect, we adjust the color, contour, filter, and sharpness of the images. After a qualitative analysis of the image characteristics, binary processing is performed on the SEM images, and the original image is converted into a binary image for pore and particle identification. The binary processing results are shown in Fig. 7.

In Fig. 7, the black and white colors represent soil particles and pores, respectively. Image threshold segmentation is key for accurately identifying soil particles and pores. In this study, a manual adjustment method is employed to perform threshold segmentation on the microimages. After binary image segmentation, the binary image data is extracted and analyzed, including the particle shape, pore size, and quantity.

The surface morphology was observed at medium magnification of × 2000. For better analysis of the variations in pores, the pores in the saline soil were divided into four categories on the basis of the loess pore classification proposed by Lei and Cui (Lei 1985; Cui and Tang 2010): minipores ($D < 2$ μm), micropores (2 μm < D < 8 μm), mesopores (8 μm < D < 32 μm), and macropores ($D > 32$ μm).

IPP software was used to analyze the SEM images. In the results, no minipores were found; the minimum pore size was 2.342 μm, which falls into the category of micropores. Figure 8 shows that the number of micropores increased as the Na_2SO_4 content increased, whereas pores with diameters of greater than 8 μm decreased in number with increasing Na_2SO_4 content. Among three types of pores observed, the content of micropores was greatest, ranging from 68 to 74%; the content of macropores was lowest, ranging from 2.1 to 2.9%.

In Fig. 9, it can be seen that macropores accounted for a large proportion of the total pore area. The pore area statistics generated by the IPP software indicate that although small pores occurred in the greatest number, they accounted for the smallest proportion of the total pore area. The distribution trend of pore area is almost opposite to the pore number, and

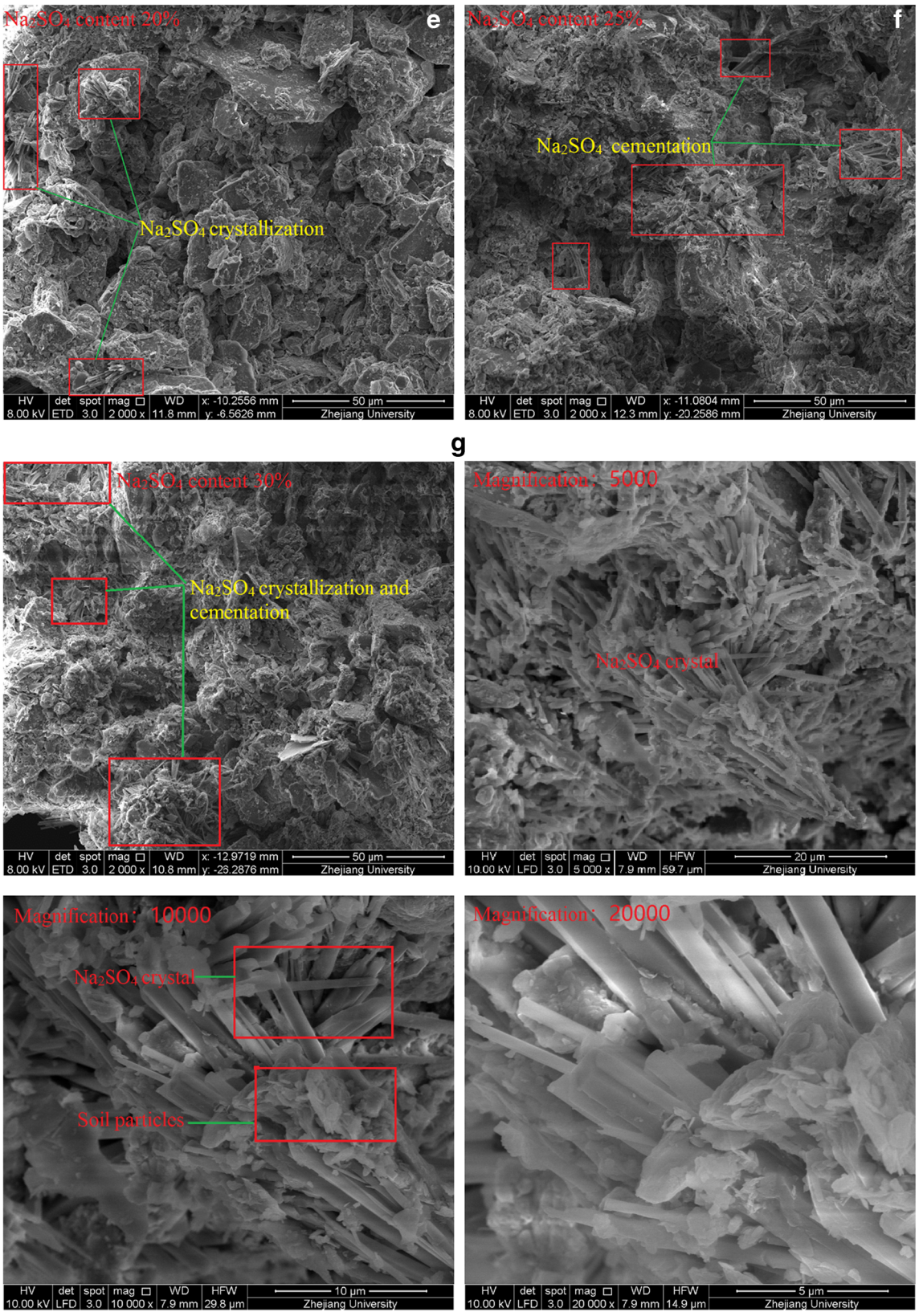

Fig. 6 (continued)

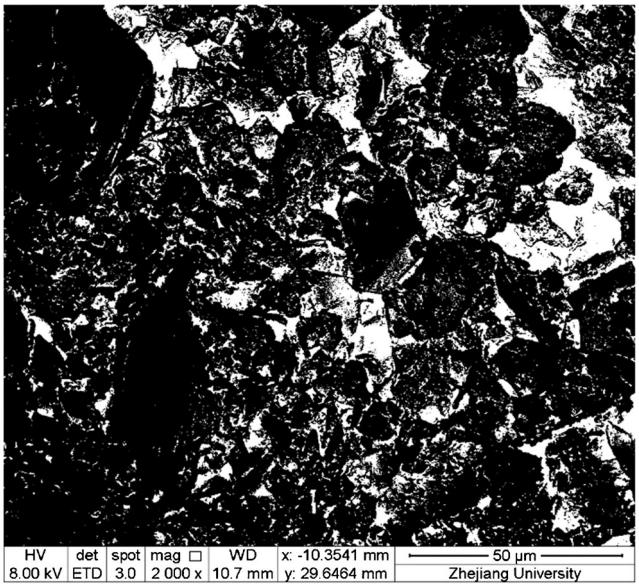

Fig. 7 Binary plot of a saline soil specimen with Na_2SO_4 content of 2%

pore area of saline soil is mainly determined by large and medium pores. With the increase of Na_2SO_4 content, the macropore area decreases, and the minipore and mesopore areas increase.

Discussions

The microstructure of soil determines its engineering properties, and the special mechanical properties of saline soil are also determined by its microstructure. Saline soil is a kind of special soil that is sensitive to the environment. Under certain conditions, the phase state and quantity of soluble crystalline salt will change. Soluble crystalline salt determines the

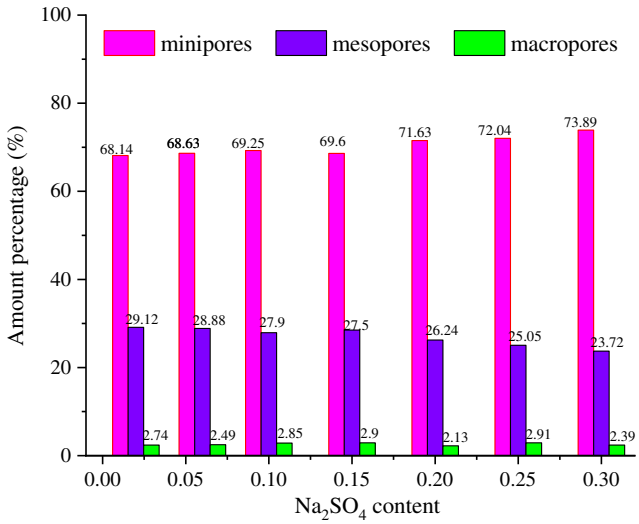

Fig. 8 Quantity percentage content of pores with different Na_2SO_4 contents

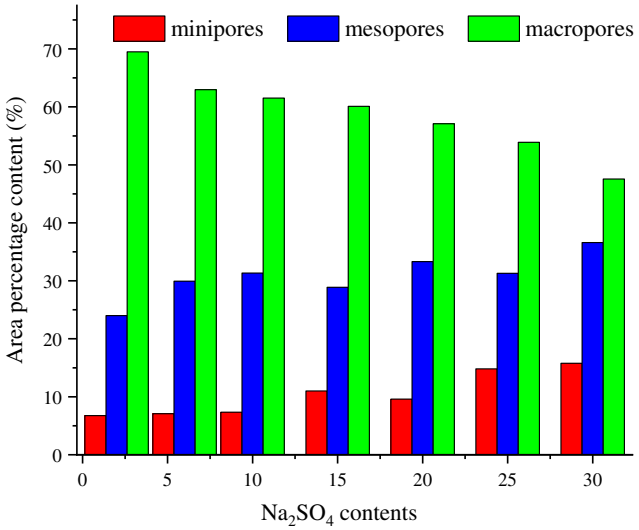

Fig. 9 Area percentage content of pores with different Na_2SO_4 contents

microstructure characteristics such as particle connection, compactness, pore size, morphology, and arrangement, which makes saline soil have unstable engineering characteristics.

In this paper, we carried out a series of resonance column test and electron microscope scanning test with different Na_2SO_4 content to explain the dynamic characteristics of saline soil from its microstructure. Results showed that when dry density and moisture content are the same, G_0 increases with the increase of Na_2SO_4 content, which is related to the crystallization of Na_2SO_4 in water. This occurs because anhydrous sodium sulfate crystallizes when it contacts water through the following reaction:

$$Na_2SO_4 + 10H_2O \rightarrow Na_2SO_4 \cdot 10H_2O \quad (7)$$

During crystallization of sodium sulfate, the volume expands by a factor of 3.11. The newly formed crystal fills in the pores of the particles, which enhances the biting force between particles. With the increase of Na_2SO_4 content, the cementation between particles is enhanced, which is consistent with Liu's (Liu and Zhang 2014) results.

Conclusions

This study experimentally investigated the shear modulus (G_0) of reconstituted saline soil, focusing on elucidating the effects of the dry density and Na_2SO_4 content. A series of saline soils with different gradations were tested, while the sodium sulfate content was well controlled, and a detailed analysis of the test results was presented in conjunction with SEM observations. An empirical equation accounting for these effects was derived based on Hardin's formula. The main conclusions of this study are summarized as follows:

1. G_0 increases with increasing confining pressure and dry density. This occurs because increasing the dry density

and confining pressure results in more soil particles per unit volume. As the dislocation between particles tends to be difficult, the shear modulus increases.

2. Taking the dry density as the state variable, the parameters of the Hardin equation are fit, and fitting parameters A and n are obtained under different dry density conditions. Using the Na_2SO_4 content as the state variable, Hardin's equation is modified to enable proper consideration of the influence of the Na_2SO_4 content on the prediction of G_0.
3. In general, G_0 increases with the Na_2SO_4 content. The underlying reason behind this phenomenon is likely that anhydrous sodium sulfate crystallizes and expands to form $Na_2SO_4{\cdot}10H_2O$ after encountering water. The newly formed crystals then fill in the pores of the particles, which enhances the biting force between particles. On the other hand, with increasing salt content, the cementation of salt crystals gradually replaces the contact between soil particles to become the dominant effect on the shear modulus of the saline soil. The inflection point in the sodium sulfate content with a significant change in the shear modulus is 20%.
4. The microstructure of the saline soil varies with different salt contents. When the salt content is low, the soil particles are in contact with each other, and the salt crystals are insufficient for effective cementation. With an increase in the salt content, the microstructure of the saline soil gradually transitions sequentially from edge-to-edge contact to edge-to-surface contact, a surface-to-surface contact skeleton structure, and a dense skeleton structure composed of particle pores filled with salt crystals.

Acknowledgments Thank you to the anonymous reviewers for their valuable feedback on the manuscript.

Author contributions XG.W contributed to the data analysis and manuscript writing. LJ.Z. proposed the main structure of this study. TD, X.Z, D, and SH, H. provided useful advice and revised the manuscript. All of the authors read and approved the final manuscript.

Funding This work was supported by the State Key Program of the Natural Science Foundation of China (grant number 51641903) and the University of Tarim President Fund (TDZKQN201705).

Compliance with ethical standards

Conflict of interest The authors declare that they have no conflict of interest

References

Al-Mukhtar M, Khattab S, Alcover J (2012) Microstructure and geotechnical properties of lime-treated expansive clayey soil. Eng Geol 139–140:17–27. https://doi.org/10.1016/j.enggeo.2012.04.004

Cui ZD, Tang YQ (2010) Land subsidence and pore structureof soils caused by the high-rise building group through centrifuge model test. Eng Geol 113(1–4):44–52

Drnevich VP, Hall JR, Richart J (1967) Effects of amplitude of vibration on the shear modulus of sand. In: Proceedings of the international symposium on wave propagation and dynamic properties of earth materials albuquerque. University of New Mexico Press, Albuquerque

Dutta TT, Saride S, Jallu M (2017) Effect of saturation on dynamic properties of compacted clay in a resonant column test. Geomech Geoeng Int J 12(3):181–190

Gao Y, Hui Q, Xinyan L, Jie C (2018) Effects of lime treatment on the hydraulic conductivity and microstructure of loess. Environ Earth Sci 77(14):1–15. https://doi.org/10.1007/s12665-018-7715-9

Hall JR Jr, Richart FE Jr (1963) Discussion of elastic wave energy in granular soils. J Soil Mech Found Div ASCE 89(SM6):27–56

Hardin BO, Black WL (1968) Vibration modulus of normally consolidated clays. J Soil Mech Found Div ASCE 92(SM2):353–369

Hardin BO, Drnevich VP (1972) Shear modulus and damping in soils: design equations and curves. J Soil Mech Found Div ASCE 98(7): 667–692

Iwasaki T, Tatsuoka F (1977) Effect of grain size and grading on dynamic shear moduli of sand. Soils Found 17(3):19–35

Iwasaki T, Tatsuoka F, Takagi Y (1978) Shear moduli of sands under cyclic tortional shear loading. Soils Found 18(1):39–56

Jafarian Y, Haddad A, Javdanian H (2014) Predictive model for normalized shear modulus of cohesive soils. Acta Geodyn Geomater 11(1): 89–100

Kokusho T (1980) Cyclic triaxial test of dynamic soil properties for wide strain range. Soils Found 20:45–60

Lei XY (1985) Pore distribution characteristics of loess in Longdong, north of Shaanxi province. Chin Sci Bull 03:206–209 (in Chinese)

Li M, Chai S et al (2016) Effect of chlorine salt on the physical and mechanical properties of inshore saline soil treated with lime. Soils Found 56(3):327–335. https://doi.org/10.1016/j.sandf.2016.04.001

Liu J, Zhang L (2014) The microstructure characters of saline soil in Qarhan Salt Lake area and its behaviors of mechanics and compressive strength. Arab J Sci Eng 39(12):8649–8658. https://doi.org/10.1007/s13369-014-1410-2

Liu Z, Liu F, Ma F, Wang M, Bai X, Zheng Y, Huang Y, Zhang G (2016) Collapsibility, composition, and microstructure of loess in China. Can Geotech J 53(4):673–686

Liu X, Zhang N et al (2019) Effects of sand and water contents on the small-strain shear modulus of loess. Eng Geol 260. https://doi.org/10.1016/j.enggeo.2019.10520220.T.T

Nie Y, Laun M, Tang X (2008) Study on hollow cylinder torsional shear of dynamic properties of two soils. Electron J Geotech Eng 13:1–11

Presti DCFL, Jamiolkowski M, Pallara O, Cavallaro A, Pedroni S (1997) Shear modulus and damping of soils. Geotechnique 47(3):603–617

Senetakis K, Anastasiadis A, Pitilakis K, Coop MR (2013) The dynamics of a pumice granular soil in dry state under isotropic resonant column testing. Soil Dyn Earthq Eng 45:70–79

Tatsuoka F, Iwasaki T, Takagi Y (1978) Hysteretic damping of sands under cyclic loading and its relation to shear modulus. Soils Found 18(2):25–40

Wichtmann T, Triantafyllidis T (2009) Influence of the grain-size distribution curve of quartz sand on the small strain shear modulus G_{max}. J Geotech Geoenviron 135(10):1404–1418

Wichtmann T, Triantafyllidis T (2013) Effect of uniformity coefficient on G/Gmax and damping ratio of uniform to well-graded quartz sands. J Geotech Geoenviron 139(1):59–72

Xu YZ (1993) Saline soil foundation. China Construction Industry Press

Yang J, Liu X (2016) Shear wave velocity and stiffness of sand: the role of non-plastic fines. Géotechnique 66(6):500–514